

Bioactivity Assessment of 8-Hydroxyquinoline and Monosodium Glutamate Mixed Ligand Copper Complex: Experimental and Computational

Mercy Bamigboye^{1a*}, Ayuba Mustapha^{1b} and Friday Danjuma^{1c}¹Department of Industrial Chemistry, Faculty of Physical Sciences, University of Ilorin, Ilorin, Nigeria.^bE-mail: ayuba.mustapha@biomedicalng.com, ^cE-mail: fridaymeschachdanjuma@gmail.com^{a*} Corresponding author: obaleye.mo@unilorin.edu.ng

Received: 2024-9-5, Revised: 2024-09-23, Accepted: 2024-10-17, Published: 2024-12-31

Abstract—The search for substances with biological activity is a prime responsibility of researchers. Coordination compounds with pharmacological activity have been essential and indispensable, especially to humans, especially organic-inorganic hybrid complexes. 8-hydroxyquinoline and Monosodium glutamate ligands were used to synthesize the copper complex by simple one-pot mixing at 35 °C. This formed complex was analysed by microanalytical, spectral, thermal, and computational techniques to characterize its formula and structure. Antimicrobial and *In-silico* activity was also determined. FT-IR spectroscopy revealed that the complex coordinated through the O-H and N-pyridine ring of Hydroxyquinoline/hydroxyl of the glutamic, confirming the suggestion of the bidentate nature of each coordinating ligand via ON/O ends. Square-planar geometry was posited for Cu, and its decomposition was observed to have decomposed around 471 °C. The proposed structure of the complex was optimised using DFT calculations, and *In-silico* was assessed. Target prediction, molecular docking, and ADME programs were used to evaluate the biological activity of the complex towards receptors in *homo sapiens specie*. In all assessments, docking scores indicated a high activity of the Cu complex as the maximum spontaneity was observed in the binding energy for the complex as an antimicrobial agent. *In-vitro* antimicrobial study for the complexes against six species: *Staphylococcus aureus*, *Bacillus subtilis*, *Escherichia coli*, *Pseudomonas aeruginosa*, *Salmonella typhi* and *Clostridium botulinum*, with maximum bactericidal effect observed in Cu complex against at 22 ± 2.72 mm at 250mg/mL profiling dosage demonstrating its potential as a pharmacological agent.

Keywords—8-Hydroxyquinoline, Glutamate, Antimicrobial activity, DFT calculations, Molecular docking, ADME studies, Bioisosterism.

I. INTRODUCTION

The search for alternative bioactive agents is attracting increasing scientific interest. Natural and synthetic products are sources of several substances with proven biological activities, including antimicrobial activity [1,2]. The relevance of the search is due to the widespread occurrence of significant diseases such as cardiovascular, infectious, oncological, and neurodegenerative ailments [2-7] Intending to provide an efficacious and safe pharmaceutical product,

added substances are often incorporated into a design formula to maintain or enhance attributes and stability [8], heteroleptic transition metal amino acid complexes are dynamic platforms for accessing a multicomponent system with unique structures, properties, and emergent functions [9]. Among the heterocyclics, compounds containing 8-Hydroxyquinoline (8-HQ), an alkaloid, exhibit a broad range of multifunctional and diverse biological activities and therapeutic potential, including antioxidant, antifungal, antimicrobial, and anticancer effects. Other medicinal properties held by 8HQ include anti-neurodegenerative, anti-inflammatory, and anti-diabetic activities [10-13]. This study is aimed at bridging experimental and computational chemistry to developing and accessing novel metal complexes with potential antimicrobial properties. The findings could contribute to the development of new antimicrobial agents and provide a framework for future research in the field of bioinorganic chemistry. The biological activity of the synthesised complex was assessed experimentally, as well as in-silico, where the pharmacokinetics, drug-likeness, and molecular docking studies were evaluated.

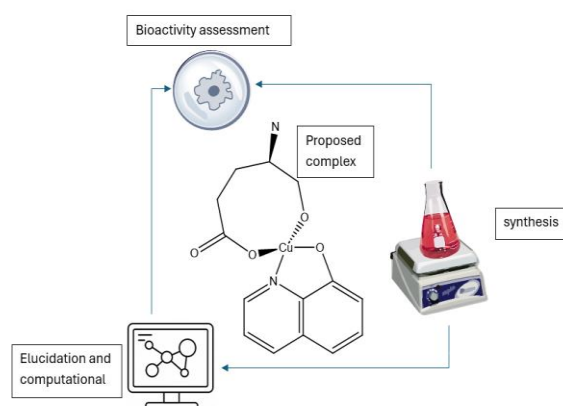


Fig. 1: Graphical illustration of the complex

II. EXPERIMENTAL

A. Materials and Methods

The chemicals used to synthesize the mixed ligand complex were monosodium glutamate, 8-hydroxyquinoline, copper (II) chloride, ethanol (absolute), and distilled water, purchased commercially without further purification. Analar DMSO (99%) was the solvent used to dissolve the complex for antimicrobial activity, specific conductivity and UV-Vis measurements. DMF solvent was also used for the solubility test.

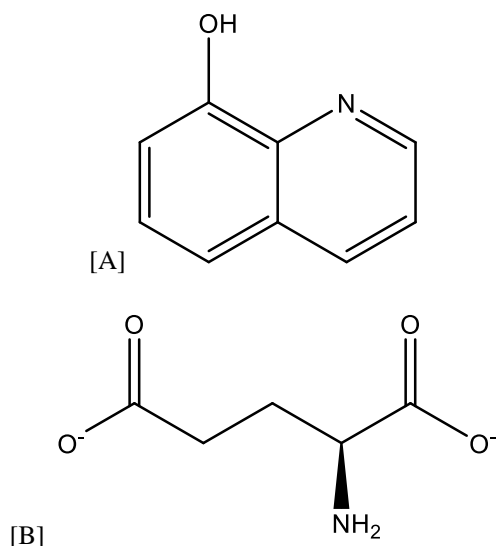


Fig.2: Ligand structures [A] 8-hydroxyquinoline [B] glutamate ion.

B. Synthesis of Complex

The complex was synthesized with slight modifications to the reported method [14]. Metal II salt (0.17 g, 1 mmol) was dissolved in distilled water (10 mL). Then equimolar amounts of Glutamate and 8-HQ (1 mmol each, 0.17 g glutamate, and 0.15g 8-HQ) were dissolved separately in distilled water and ethanol, respectively, and simultaneously added with constant stirring at 35 °C to the metal salt solution. This addition gives an equal chance for the ligands to coordinate with the metal. The reaction mixture was mixed for 1 hour at 300 rpm and held at 35 °C. The resultant mint-green precipitate was washed with 50 % ethanol solution thrice, filtered, and dried in a desiccator for 72 hours.

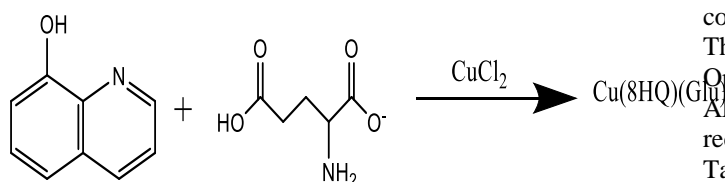


Fig. 3: Synthetic path for the complex.

C. Equipment

Conductometric measurement was taken using an industrial conductivity meter, DDS-307 digital meters for a 1 mmol complex in DMSO, Infrared spectrum scan in the region 4000 – 400 cm⁻¹ was measured with FTIR-8700 SHIMADZU Fourier Transform InfraRed spectrophotometer, and the SEM micrograph imaging was collected from Phenom Prox model microscope. The XRD

Rigaku MiniFlex 600 XRD diffractometer produced the XRD spectrum, the Quantachrome NOVA4200e analyser was used to take the BET studies, the T70 double-beam spectrophotometer read the UV-Vis spectral behaviour of the complex, and the TGA-Q500 to produce a spectrum of mass previously dried and with a particle size less than 50 µm against temperature scanning to 900 °C.

D. In vitro Assessment

Using the described Agar Well diffusion method [15,16], the antimicrobial activity of the complex and ligands was investigated by measuring the zone of inhibition using DMSO as a control against *Staphylococcus aureus*, *Clostridium botulinum*, *Bacillus subtilis*, *Escherichia coli*, *Pseudomonas aeruginosa*, and *Salmonella typhi*. The minimum lethal concentration (MLC), also referred to as the Minimum Bactericidal Concentration (MBC), was assessed for the samples. The MLC is defined as the lowest concentration of an antimicrobial agent necessary to kill 98-99.9% of the final inoculum after 24 hours, as specified by the standardized conditions in the Clinical Laboratory and Scientific Institute (CLSI) M26-A guidelines. [17]. A stock preparation of solution of 500 mg/mL in DMSO was used to estimate the MIC and MBC.

E. Structural and Pharmacokinetics Optimization

In complementing the experimental characterisation techniques, DFT calculations using the molecular dynamics simulation program, Gaussian 09, were used for electronic structure modeling to project and analyse insightful properties of the synthesised complex. Optimisation and calculations ran the valence double zeta polarising basis set, 6-31G*, and Becke3-Lee-Yang-Parr, B3LYP. Gauss-View and Gauss-Sum software were used to evaluate the generated computational files (log and chk) to retrieve all physical properties [18].

F. In silico Assessment

The optimised structure was then subjected to Swiss Target Prediction and screened for human-microbe relationship activity [19]. Target Prediction estimates the most probable macromolecular target of a small molecule assumed as bioactive.

Molecular docking studies were conducted to gain insights into the microbial activity of the synthesized complex. These studies provided an accurate prediction of the biological behaviour of the complex under investigation. This was used to establish a correlation between the computational and experimental behaviour of the complex. The chosen algorithm for this study was the Molecular Operating Environment (MOE, v2022.02), and Swiss ADME to confirm oral bioavailability. Three protein receptors (1B87, 1YAK, and 8CXT) were obtained based on Target Prediction, and three more receptors (3NZS, 3HY3, and 8JZN) were obtained from a literary source [18,20]. These receptors were characterized with the PDB database (www.rcsb.org). 1B87, 1YAK, 8CXT, and 8JZN are key protein receptors found in *Enterococcus faecium*, *Bacillus subtilis*, *Clostridium difficile*, and *Saccharomyces cerevisiae*, respectively. 3NZS, a kinase receptor, is essential for cellular activities. 3HY3 is also a kinase receptor known for the proliferation of breast cancer [18]. Inhibiting these target receptors may predicate the activity of the complex against these enzymes.

The optimised structure of the complex and receptor was entered into a docking library. Using a Triangle Matcher placement, Induced Fit refinement while combining London dG and GBVI/WSA dG functions against 30 poses. The complex was docked onto the receptor to determine its binding affinity [21,22]. The pattern for the docking operations was examined to investigate the interactions in the activity. The bond length for each interaction was determined against an effective length of 3.5 Å [23]. Swiss ADME defines the theoretical values of the physicochemical indexes that describe the pharmacokinetics (ADME) and drug-likeness of the synthesized complex meant for oral consumption. As a function of the Absorption-Distribution-Metabolism-Elimination (ADME), the bioavailability score and map of the complex were generated using Lipinski's rule of five (RO5) and Veber rules [24,25]. The hypothetical polarity of surface area (TPSA), solubility (log *S*), and unsaturation ratio depending on sp³ hybridized carbon and flexible bonds were used in the bioavailability mapping to assess the drug-likeness of the complex. Other chemical descriptors crucial for supporting pharmacokinetics in organisms and tissues, such as solubility in aqueous solution and the partition coefficient between n-octanol and water (log *P* o/w), were also identified and analyzed [18].

III. RESULTS AND DISCUSSION

A. Analytical and Spectroscopic studies

Upon completion of synthesis, the yield and conductivity of the complex were measured to be 87.3 % and 7.09 μS/cm, respectively. The synthetic route yielded an appreciable amount of the copper complex, and the complex was evaluated to be electrolytic in nature. The complex was also found to be less soluble in polar solvents but soluble in DMSO and DMF. The thermogravimetric data indicated that the complex completely decomposed at 471 °C, exhibiting exothermic peaks. The completion of the TG/DTA phase recorded the degradation of the complex, resulting in a metal oxide composition. To grow single crystals of the complex, the filtrate was left to slowly evaporate. After 19 days, needle-like crystals were obtained but were not captured analytically in this study. However, the precipitate was characterized by FTIR, UV-Vis spectroscopy. The IR frequencies of the ligands and synthesized complex have been reported in the table below. The assignment has been based on literature and computational values obtained for the ligands and complexes. The free ligands are characterized by the presence of O-H groups. The registered peaks around 3350 cm⁻¹ represented the absorption for the O-H peaks in the 8HQ and Glu ligands. The ligands also record a C-N bending vibration at 1089 and 1067 cm⁻¹ respectively, with a C=N at 1600 cm⁻¹ in the 8HQ ligand, a similar occurrence reported in [14, 30]

With the complex, the appearance of the ν(M-O/M-N) bands and the disappearance of the ν(O-H/N-H) band previously sighted in the free ligands supported the coordination of the glutamate and 8-Hydroxyquinoline through the O-H/O⁻ oxygen and the N-nitrogen. Also, the complexes demonstrated aromatic and aliphatic character as portrayed by the ligands to support the coordination claim. At 3317 cm⁻¹, the upheld the N-H stretching in the glutamate end of the complex. Band resulting from M-O to confirm coordination was observed for 568.30, cm⁻¹ for the complex. In addition to ν(M-O), the spectrum also reflected another

peak, ν(M-N), at 470.55 cm⁻¹ due to the coordination of the metal via the Nitrogen atom. These attributes found in the complex were not found in the ligands confirming the formation of the complex.

Table 1: Key absorption bands for the ligands and complex.

Complex	ν(C-O)	ν(C-H)	ν(C-H)	ν(C=O)	ν(C=C)	ν(M-O)		
Cu(Glu)(8-HQ)	1091.51	3043.12	2925.48	1611.11	1454.06	568.30		
(L)	ν(C=C)	ν(O-H)	ν(N-H)	ν(C-H)	ν(C=N)	ν(N=C=O)	ν(N-C-O)	ν(C-N)
Glu	-	3350	1372	818	-	1600	1260	1067
8-HQ	1450	3355	-	801	1600	-	1275	1089

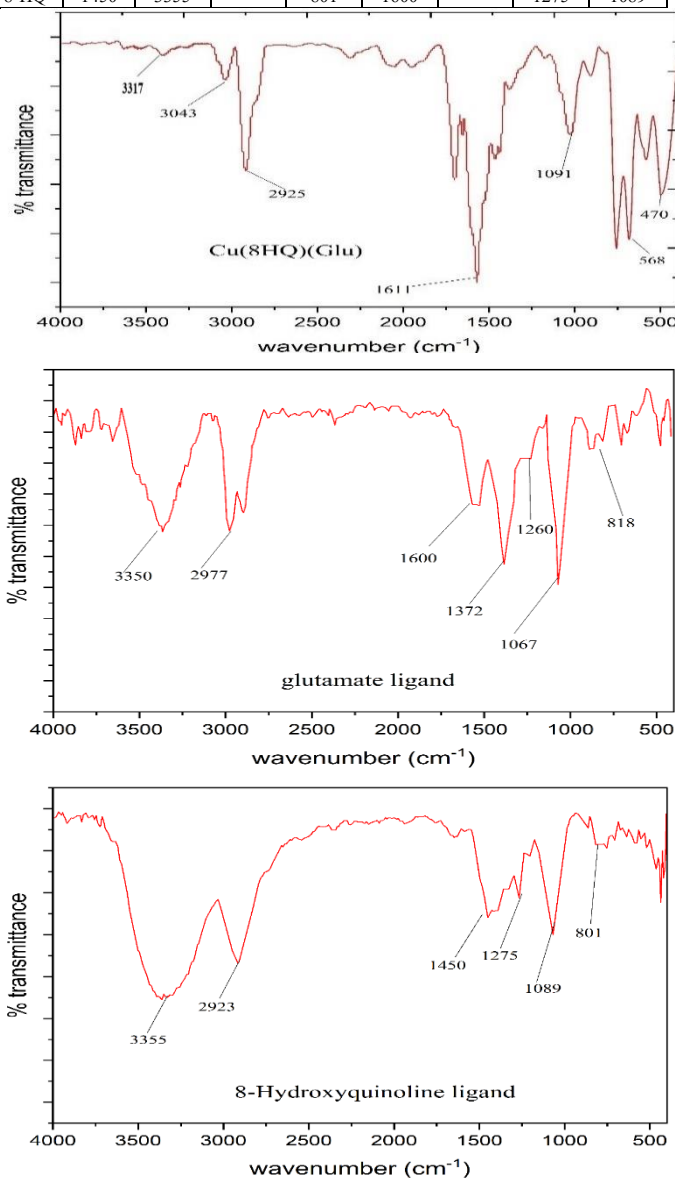


Fig. 4: FTIR spectra of the ligands and complex.

The UV-Vis spectrum (Figure 5) of the complex offered valuable insights into the electronic structure and coordination environments of the transition metal. A yellow colour was obtained upon dissolution in DMSO, highlighting the effect of the chromophoric influence of the 8HQ ligand in the ligand field interaction with the metal [26]. The complex showed distinct peaks at 260 and 295 nm, corresponding to π-π* and n-π* electronic transitions (ligand-centered interactions), indicative of the aromatic/conjugated systems and heteroatom interactions in

the 8HQ. A slight inflexion was observed between 390 – 400 nm, which may denote the d-d transition. The distinct peak denoted as 445 nm is attributed to the charge transfer (CT) transition, likely metal-to-ligand charge transfer (MLCT) over LMCT. In an MLCT transition, the metal-centered orbital (usually the d-orbital) transfers electrons to the ligand-centered orbital (usually the π^* orbital) [26,27,28]. The presence of these transitions indicates that the suggested geometry of the Cu complex is square planar.

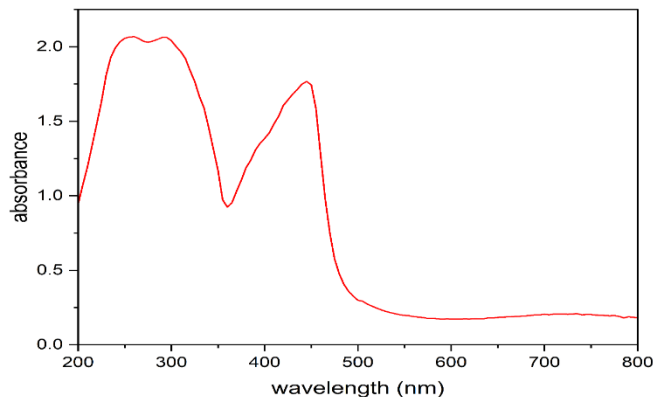


Fig. 5: UV-Vis spectrum of the complex.

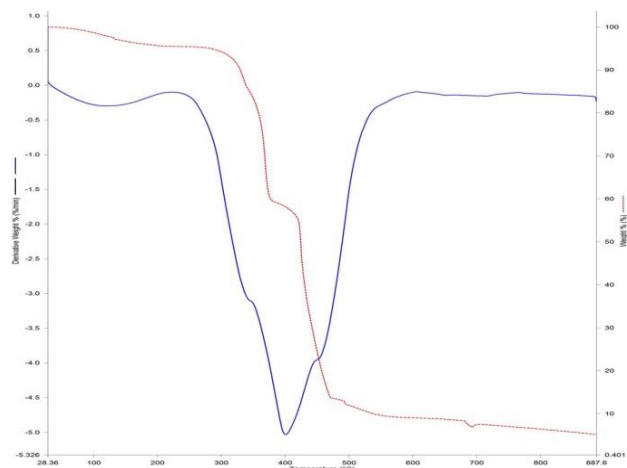


Fig. 6: Thermogravimetric decomposition pattern of the complex.

B. SEM, XRD and BET Analyses

The SEM images (Figure 7^a) provided detailed information on the structural, surface morphology, and particle size of the synthesized complex in an ethanol-water solvent formation system. Morphological analysis of the copper complex revealed a highly textured fibrous and porous structure with irregularly shaped particles and significant surface roughness. The observed morphology suggests heterogeneous nucleation and growth processes caused by water-ethanol and container interactions, indicative of the complex formation. The porous and fibrous nature of the formed substance could be attributed to the interaction between an organic and inorganic phase component, leading to a high surface area. The synthesized complex's unique structural and compositional properties make it suitable for catalytic applications and hold potential for pharmaceutical use [30].

XRD analysis was conducted on the Cu complex using Cu/K α radiation under $10^\circ < 2\theta < 80^\circ$ range at 25 °C [23]. The XRD patterns revealed several distinct diffraction

peaks, each corresponding to various crystalline phases within the sample, particularly notable at 2θ at 7.33, 8.74, 11.57, and 21.60 ° for the Cu complex. The highest intensity peaks, 7.33 ° and 8.74 °, suggest dominant phases within the sample, indicating a high degree of crystallinity with the synthesized compounds. Other peaks and well-defined phases also contribute to the overall crystalline structure but are less intense. The crystallite size, calculated using the Scherrer equation, ranged from 18.4 to 39.3 nm, averaging 28.975 nm, which indicated a well-defined nano-crystalline structure of the complex. The presence of sharp, intense, and distinct peaks suggests that the Cu sample is highly crystalline, with well-ordered crystal lattices within the complex. The presence of a high degree of crystallinity and ordered phases suggest structural integrity under several conditions critical for consistent performance [29].

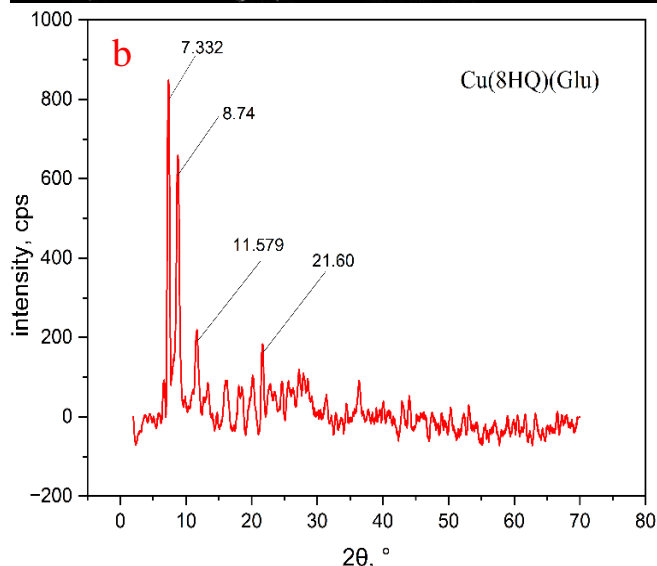
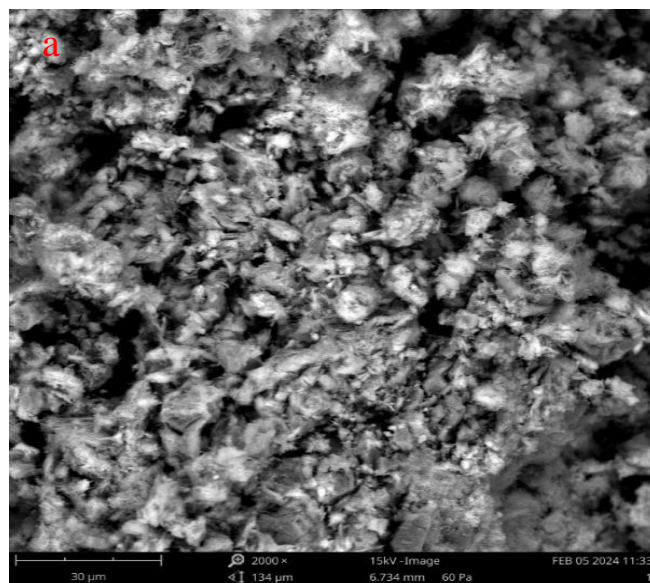


Fig. 7: ^aSEM and ^bXRD imaging for the complex.

The Specific Surface Area obtained from the Multi-point BET and DA models revealed that the copper complex has a surface area of 415.961 m²/g, a micropore size of 2.940 nm, and a pore volume of 0.379 cc/g, contrasted to 474.818 m²/g, 2.136 nm and 0.232 cc/g respectively revealed by the BJH model. The surface area determined by Langmuir

analysis revealed 2994.173 m²/g indicating the presence of a multilayer adsorption.

C. Antimicrobial Activity

The synthesized complex was screened against the standard gram-positive and gram-negative bacteria. The complex exhibited varying degrees of antibacterial activity against the six organisms. The Copper complex was sensitive against *S. aureus*, *P. aeruginosa*, *C. botulinum*, and *B. subtilis*, but resistance was observed in *S. typhi* and *E. coli*. The 8HQ ligand was found to be sensitive to all organisms, while the Glu ligand was resistant to *E. coli* but active against others.

The Cu complex recorded the highest antimicrobial activity against *B. subtilis* with a 22.875±3.13 mm zone of inhibition followed by *S. aureus* with 17.875±2.03 mm zone of inhibition, *P. aeruginosa* with a 15.375±1.52 mm zone of inhibition and *C. botulinum* accounting for the least 11.975±1.02 mm zone of inhibition. There was a statistically significant difference (p<0.05) in the antimicrobial activity across the test bacteria in the sample.

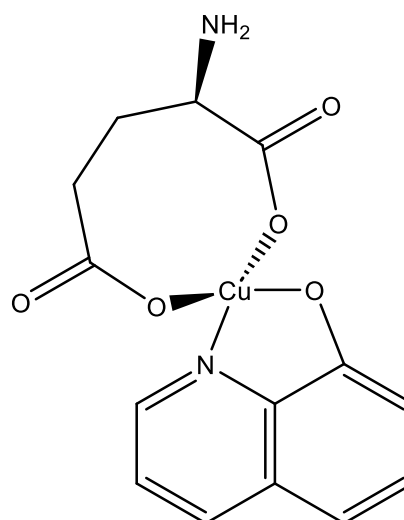


Fig. 9: Proposed structure for the metal complex.

DFT Optimization and Stability: The data in Table 3 was obtained after running DFT calculations.

Data from DFT calculations of the structures indicated that

Table 2: Antibacterial profile for the complex

Sample code	Differential Activity against Test-organism					
	<i>S. aureus</i>	<i>P. aeruginosa</i>	<i>S. typhi</i>	<i>E. coli</i>	<i>C. botulinum</i>	<i>B. subtilis</i>
complex	17.875±2.03 ^d	15.375±1.52 ^c	0.000±0.00 ^a	0.000±0.00 ^a	11.975±1.02 ^b	22.875±3.12 ^c
Glu	13.375±1.73 ^c	15.625±2.05 ^d	8.250±0.72 ^b	10.775±1.12 ^{bc}	0.000±0.00 ^a	22.875±3.27 ^c
8HQ	11.125±0.95 ^c	16.775±1.53 ^d	7.750±0.52 ^b	0.000±0.00 ^a	10.875±0.87 ^c	20.275±2.17 ^c
DMSO	22.55±4.05 ^d	21.70±3.57 ^c	20.50±3.21 ^b	18.75±2.72 ^a	23.25±4.72 ^c	21.55±3.49 ^c

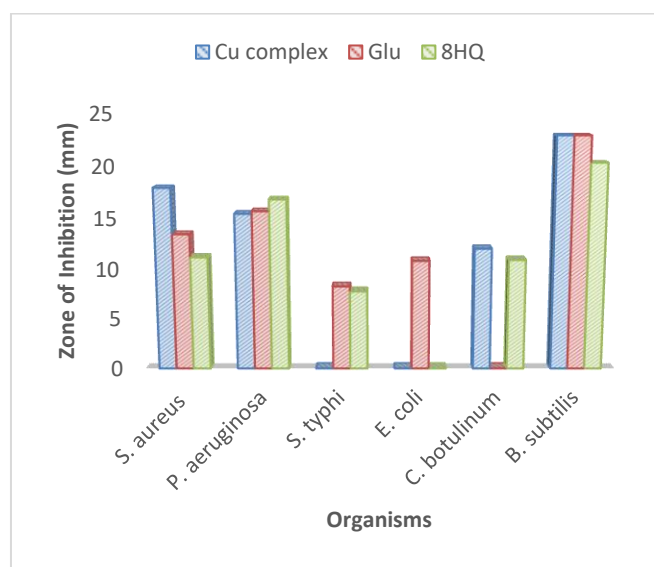


Fig. 8: antibacterial screen of the ligands and complex.

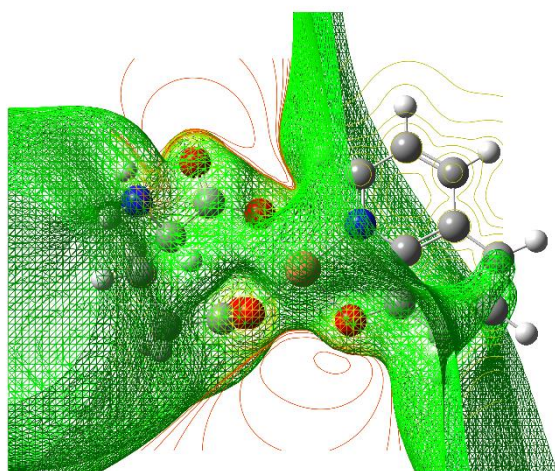
D. In Silico Assessment

Structure Proposition: Using data obtained from characterization, the structure in Figure 8 was proposed for the Copper complex.

the ligands exhibit high nucleophilicity, as reflected in the atomic Mulliken charges of N and O in 8HQ and Glu [14]. However, these charges were slightly reduced in the Copper complex.

The optimized complex posits the most accurate orientation of the coordinating atoms from the mixed ligands used and, therefore, support their coordination to the Cu (II) without bond strain or twisting of the functional groups. This is easily observed in the bond lengths obtained from the calculation. An elongation of the coordinating bonds was observed but within the range of 0.9 – 3 Å from complexation. Bond angles estimated for the complexes on the coordination centre revealed that the bond angle for the Cu complex is approximately 90° in the singlet state, supporting the square planar for the Cu complex, respectively.

The HOMO and LUMO imaging were obtained from the optimized structure. The contoured orbitals appear over the functional groups of the complex, highlighting that the electronic transition is primarily confined to the coordinating functional groups. The shape of these orbitals exhibited significant changes compared to those in the two complexes formed by the ligands.



Cu complex
ESP density: $-1.869e-2$ to $1.869e-2$

Fig. 10: Electrostatic Potential/Electron density iso-surface imaging of the complex.

Electrostatic potential mapping using the electron density measurements revealed the presence of a positive and negative iso-value (yellow=positive and red=negative) represented in Figure 10. The iso-surface values in the Cu complex, ranging from $-1.869e-2$ to $1.869e2$, indicate the ability to absorb electrons from the environment. If the complex interacts with amino acids in biological systems, they could potentially interact with additional functional groups. This suggests that the Cu complex may exhibit a biological activity [14].

Moreover, in these complexes, yellow or positive regions are more susceptible to nucleophilic attack, whereas red regions are more susceptible to electrophilic attack. This information is crucial for understanding how these complexes might interact with biomolecules in biological contexts, influencing their biological activity and potential applications.

Molecular docking studies: Docking studies to shed more light on the in vitro results obtained for the complexes using MOE against the chosen protein targets. Results are as shown in Table 4.

The binding scores of the complex were higher than those observed in the ligands, which may attributed to a higher number of receptor components sharing proximity with the complex than the individual ligands. However, interaction distances were slightly higher than anticipated, which may cause weaker or repulsive interactions, resulting in the binding strength being mild compared to that observed for Cefuroxime. Cefuroxime had a binding affinity of -7.91 , -9.24 , and -7.21 kcal/mol towards the 1B87, 1YAK, and 8CXT receptors, respectively. The mild interaction of the complex could be attributed to having lesser interactions with the receptors compared to that exhibited by the antibiotic [31].

However, when pitted against 8JZN, an antifungal receptor, the complex recorded -6.4434 against -6.3345 of fluconazole. This demonstrated an almost equivalent action, computationally, and experiments may demonstrate this activity [31].

Table 3: Molecular docking insights for the complex.

Compound	Protein	Interaction	Distance	S (energy score)
8HQ	1B87	Arene-H	4.39	-4.4863
	1YAK	-	-	-5.0563
	8JZN	Arene-H, sidechain	4.24, 3.23	-4.6053
	8CXT	Arene-H	3.33	-4.7702
	3HY3	Arene-H	3.95	-4.9634
Glu	3NZS	Arene-H	3.96	-4.9865
	1B87	Sidechain	3.19	-4.8910
	1YAK	Sidechain	3.38	-5.0164
	8JZN	Sidechain	3.97	-4.8276
	8CXT	Sidechain	3.88	-4.8801
Cu(8HQ)(Glu)	3HY3	Sidechain	2.94	-4.9623
	3NZS	Sidechain, backbone	2.89, 2.87	-4.9522
	1B87	Arene-H	3.81	-6.6891
	1YAK	Arene-H	3.44	-6.4714
	8JZN	Arene-H, sidechain	2.82, 3.97	-6.4434
	8CXT	Arene-H, sidechain	4.64, 3.53	-6.5446
	3HY3	Arene-H	4.60	-6.6478
	3NZS	Arene-H	3.98	-6.9782

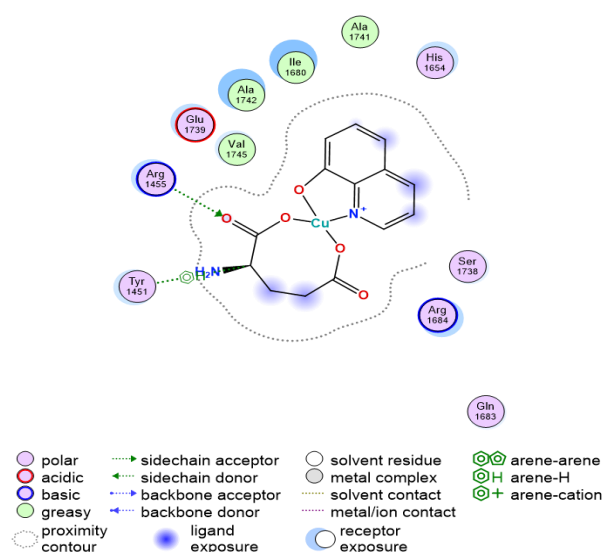


Fig. 11: Copper-Ligand Transferase Receptor Interaction

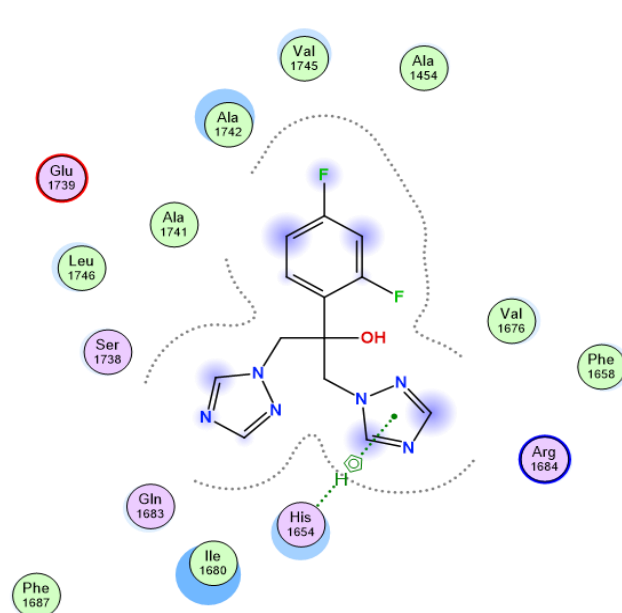
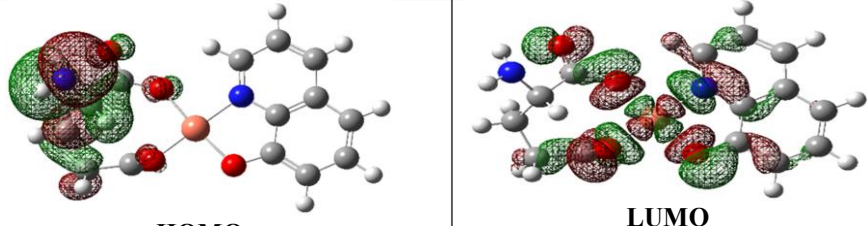
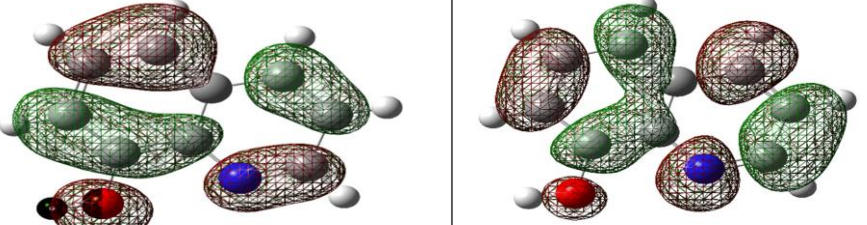
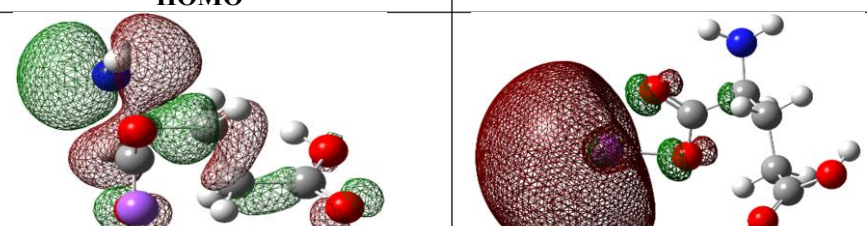


Fig. 12: Fluconazole (reference)-8JZN receptor interaction.

Table 4: Insights obtained from DFT calculations.

Compounds	Computed descriptor	Bond length (Å)	Bond angle (°)	Mullikan's charge
Copper complex	HOMO = -0.21241 eV	Cu – N ¹⁶ = 1.913	N ¹⁶ -Cu ¹⁸ -O ¹⁷ =90	N ¹⁶ = -0.705
	LUMO = -0.16014 eV	Cu – O ¹⁷ = 1.856	O ²⁰ -Cu ¹⁸ -N ¹⁶ =89	O ¹⁹ = -0.532
	Dipole moment = 5.2768 Debye	C ¹ – C ⁶ = 1.419	O ¹⁹ -Cu ¹⁸ -N ¹⁶ =178	Cu ¹⁸ = 0.951
	Formation energy = -2667 au	C – O ¹⁷ = 1.362		O ²⁶ = -0.422
	ΔE=0.05227 eV	C = O ²⁷ =1.243		O ¹⁷ = -0.616
		C ⁴ – N ¹⁶ =1.375		C ¹ = -0.125
8-Hydroxyquinoline	HOMO = -0.21499 eV	C – O = 1.382	-	N = -0.375
	LUMO = - 0.04785 eV	C = N=1.330	-	O = -0.587
	Dipole moment = 2.7542 Debye	C – N = 1.371	-	
	Formation energy = - 477.01 au		-	
Glutamic acid	HOMO = -0.20347 eV	C – O = 1.393	-	N = -0.713
	LUMO = - 0.06302 eV	C = O = 1.227	-	O = -0.556
	Dipole moment = 5.7344 Debye	C – N = 1.452	-	O = -0.596
	Formation energy = - 713.19 au		-	
		Complex		
		8HQ		
		Glu		

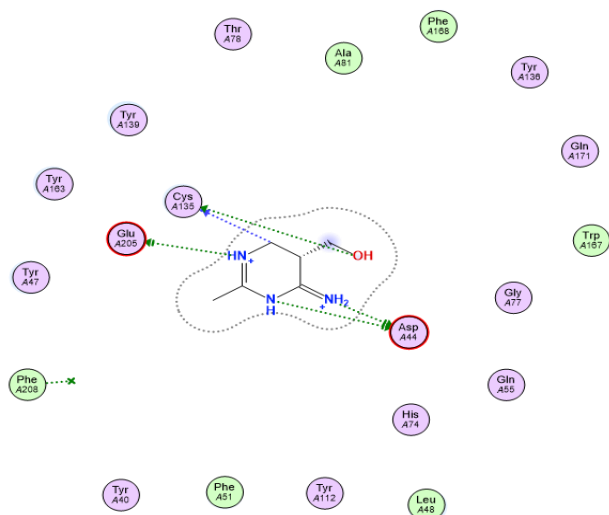
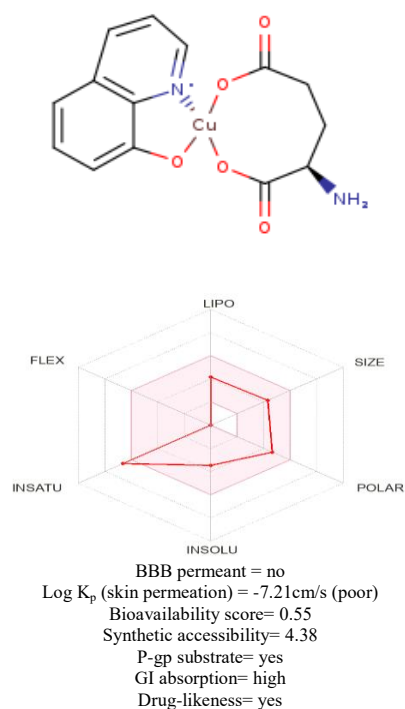


Fig. 13: Cefuroxime (reference)-1YAK receptor interaction.

ADME estimation: ADME assessment performed on the complexes provided insights into their drug-likeness and pharmacokinetics properties as given in Table 5, which are crucial in the pursuit of new drug entities.

Table 5: ADME parameters of the complex.



The pink area represents the optimal range for the indexes guiding the bioavailability of the substances if intended for oral consumption [24]. The synthetic accessibility score of drug-like molecules for virtual screening exploration expresses the ease of synthesis of molecules on a scale of 1 to 10, with 1 being easy and 10 being difficult to synthesize [32]. S.A. 4.38 of the copper complex underpins averagely easy to synthesize, which also highlights the ease of accessing starting materials for the complexes. Having

passed Lipinski's rule of five (RO5), a bioavailability score of 0.55 highlights that the bioactive substance is at least 55% available for systemic circulation in its active form while losing a considerable amount to P-gp. P-glycoprotein is an efflux transporter protein present in various tissues including the liver, kidney, intestinal epithelium, and the BBB (blood-brain-barrier) [33,34]. P-gp actively pumps the complexes back into the bloodstream or excretory pathways, thereby limiting their intracellular concentration.

Conversely, the complex is non-BBB permeant, indicating it is not intended to affect the Central Nervous System (CNS). This characteristic could be beneficial by preventing CNS side effects while targeting peripheral sites, making these compounds potential candidates for further experimental consideration [35].

The ADME assessment revealed that the complex is a potentially viable drug-likeness candidate, with five of the six indexes conforming to optimal ranges for oral bioavailability. However, the complexes exhibited a high presence of double bonds, which contributes to chemical and metabolic instability and reactivity, potentially leading to accumulation in fatty tissues during distribution. Additionally, as P-gp substrates with moderate bioavailability, higher doses might be required to achieve therapeutic levels, but this must be balanced against the risk of potential side effects [36].

The substance being a P-gp substrate with only moderate bioavailability suggests potential areas for optimization. Bioisosterism could be employed to enhance this crucial index, thereby improving the bioavailability and binding affinity of the complex. Additionally, formulation strategies or co-administration with P-gp inhibitors might be considered to further improve bioavailability [37, 38].

IV. CONCLUSIONS

Investigations into the synthesis of the mixed complex using a one-pot synthetic path were successful carried out from copper ion, 8-Hydroxyquinoline, and Glutamate ion in the ratio 2:1:1. The molecular and structural information was suggested based on spectral, analytical, and computational techniques. The copper ion bound to the bidentate ligands, resulting in the formation of square-planar geometry for the complex. Geometry optimization yielded the best structural orientation and geometric insights into the prepared complex. Evaluations of the biological activity of the complex showed certain antibacterial activity toward the test organisms, like the ligands. However, *in silico* assessments reveal a more probable use as an antifungal agent. Experimental confirmations are currently underway to assess this activity, along with investigations using obtained crystals. ADME studies have indicated a potential for structural modifications to enhance the bioavailability of the synthesized complex.

CONFLICT OF INTEREST

The authors declare that they have no conflict of interest.

REFERENCES

- [1] J. C. S. Prado, G. M. Prado, F. L. L. Aguiar, A. M. Neves, J. F. do Nascimento, F. O. M. da Silva Abreu, and R. O. dos Santos Fontenelle, "Nanoemulsions of

- plant-based bioactive compounds with antimicrobial applications: a review,” *Ciência e Natura*, vol. 46, p. e74325, Apr. 2024, doi: <https://doi.org/10.5902/2179460x74325>.
- [2] H. M. Patel, V. Bhardwaj, P. Sharma, M. N. Noolvi, S. Lohan, S. Bansal and A. Sharma, “Quinoxaline-PABA bipartite hybrid derivatization approach: Design and search for antimicrobial agents,” *Journal of Molecular Structure*, vol. 1184, pp. 562–568, May 2019, doi: <https://doi.org/10.1016/j.molstruc.2019.02.074>.
- [3] J. A. Asong, S. O. Amoo, L. J. McGaw, S. M. Nkadimeng, A. O. Aremu, and W. Otang-Mbeng, “Antimicrobial Activity, Antioxidant Potential, Cytotoxicity and Phytochemical Profiling of Four Plants Locally Used against Skin Diseases,” *Plants*, vol. 8, no. 9, p. 350, Sep. 2019, doi: <https://doi.org/10.3390/plants8090350>.
- [4] U. Anand, N. Jacobo-Herrera, A. Altemimi, and N. Lakhssassi, “A Comprehensive Review on Medicinal Plants as Antimicrobial Therapeutics: Potential Avenues of Biocompatible Drug Discovery,” *Metabolites*, vol. 9, no. 11, p. 258, Nov. 2019, doi: <https://doi.org/10.3390/metabo9110258>.
- [5] R. Mazzei, M. Leonti, S. Spadafora, A. Patitucci, and G. Tagarelli, “A review of the antimicrobial potential of herbal drugs used in popular Italian medicine (1850s–1950s) to treat bacterial skin diseases,” *Journal of Ethnopharmacology*, vol. 250, p. 112443, Mar. 2020, doi: <https://doi.org/10.1016/j.jep.2019.112443>.
- [6] N. Rivera-Yañez, C. R. Rivera-Yañez, G. Pozo-Molina, C. F. Mendez-Catala, J. Reyes-Realí, M. I. Mendoza-Ramos, A. R. Mendez-Cruz, and O. Nieto-Yanez “Effects of Propolis on Infectious Diseases of Medical Relevance,” *Biology*, vol. 10, no. 5, p. 428, May 2021, doi: <https://doi.org/10.3390/biology10050428>.
- [7] K. M. Hillgren, D. Keppler, A. A. Zur, K. M. Giacomini, B. Stieger, C. E. Cass, L. Zhang, and International Transporter Consortium, “Emerging Transporters of Clinical Importance: An Update From the International Transporter Consortium,” *Clinical Pharmacology & Therapeutics*, vol. 94, no. 1, pp. 52–63, Jul. 2013, doi: <https://doi.org/10.1038/clpt.2013.74>
- [8] G. A. Gazieva and Konstantin Chegaev, “Special Issue ‘Development and Synthesis of Biologically Active Compounds,’” *International Journal of Molecular Sciences*, vol. 25, no. 7, pp. 4015–4015, Apr. 2024, doi: <https://doi.org/10.3390/ijms25074015>.
- [9] E. Santi, I. Viera, A. Mombrú, J. Castiglioni, E. J. Baran, and M. H. Torre, “Synthesis and Characterization of Heteroleptic Copper and Zinc Complexes with Saccharinate and Aminoacids. Evaluation of SOD-like Activity of the Copper Complexes,” *Biological Trace Element Research*, vol. 143, no. 3, pp. 1843–1855, Feb. 2011, doi: <https://doi.org/10.1007/s12011-011-8992-2>.
- [10] M. Subhadip Neogi and M. Schmittel, “Dynamic heteroleptic metal-phenanthroline complexes: from structure to function,” vol. 43, no. 10, pp. 3815–3834, Feb. 2014, doi: <https://doi.org/10.1039/c3dt53570c>.
- [11] A. Cipurković, E. Horozić, S. Marić, L. Mekić, and H. Junuzović, “Metal Complexes with 8-Hydroxyquinoline: Synthesis and *In Vitro* Antimicrobial Activity,” *Open Journal of Applied Sciences*, vol. 11, no. 01, pp. 1–10, 2021, doi: <https://doi.org/10.4236/ojapps.2021.111001>.
- [12] M. A. S. Shebab, M. El-Naggar, R. A. Ismail, H. M. Kafrawy, A. Abood, S. A. Ismail, N. M. Sabry, and M. T. El Sayed, “Synthesis of Some Novel Quinolins with *In-vitro* Antimicrobial, and Antioxidant Activity,” *Current Bioactive Compounds*, vol. 16, no. 4, pp. 514–520, Feb. 2019, doi: <https://doi.org/10.2174/1573407215666190131112730>.
- [13] V. Prachayasittikul, V. Prachayasittikul, S. Prachayasittikul, and S. Ruchirawat, “8-Hydroxyquinolines: a review of their metal chelating properties and medicinal applications,” *Drug Design, Development and Therapy*, p. 1157, Oct. 2013, doi: <https://doi.org/10.2147/dddt.s49763>.
- [14] S. A. Amolegbe, S. Adewumi, C. A. Akinremi, J. F. Adediji, A. Lawal, A. O. Atayese, and J. A. Obaleye, “Iron(III) and copper(II) complexes bearing 8-quinolinol with amino-acids mixed ligands: Synthesis, characterization and antibacterial investigation,” *Arabian Journal of Chemistry*, vol. 8, no. 5, pp. 742–747, Sep. 2015, doi: <https://doi.org/10.1016/j.arabjc.2014.11.040>.
- [15] D. C. Das, S. De, S. Bhattacharya, and M. Das. “Antibacterial activity and Phytochemical analysis of *Cardanthera difformis* Druce leaf extracts from West Bengal, India.” *International Journal of phytomedicine* 5, no. 4 (2013): 446.
- [16] D. Das, B. C. Nath, P. Phukon, and S. K. Dolui, “Synthesis and evaluation of antioxidant and antibacterial behavior of CuO nanoparticles,” *Colloids and Surfaces B: Biointerfaces*, vol. 101, pp. 430–433, Jan. 2013, doi: <https://doi.org/10.1016/j.colsurfb.2012.07.002>.
- [17] M. Balouiri, M. Sadiki, and S. K. Ibsouda, “Methods for in vitro evaluating antimicrobial activity: a review,” *Journal of Pharmaceutical Analysis*, vol. 6, no. 2, pp. 71–79, Apr. 2016, doi: <https://doi.org/10.1016/j.jpha.2015.11.005>.
- [18] F. S. Alhazmi, M. Morad, Khlood Abou-Melha, and N. M. El-Metwaly, “Synthesis and Characterization of New Mixed-Ligand Complexes; Density Functional Theory, Hirshfeld, and In Silico Assays Strengthen the Bioactivity Performed In Vitro,” *ACS Omega*, vol. 8, no. 4, pp. 4220–4233, Jan. 2023, doi: <https://doi.org/10.1021/acsomega.2c07407>.
- [19] X. Wang, W. Zhao, X. Zhang, Z. Wang, C. Han, J. Xu, G. Yang, J. Peng, and Z. Li, “An integrative analysis to predict the active compounds and explore polypharmacological mechanisms of *Orthosiphon stamineus* Benth.,” *Computers in Biology and Medicine*, vol. 163, p. 107160, Sep. 2023, doi: <https://doi.org/10.1016/j.compbiomed.2023.107160>.
- [20] C.-R. Zhao, Z. L. You, D. D. Chen, J. Hang, Z. B. Wang, M. Ji, L. X. Wang, P. Zhao, J. Qiao, C. H. Yun and L. Bai, “Structure of a fungal 1,3-β-glucan synthase,” *Science Advances*, vol. 9, no. 37, Sep. 2023, doi: <https://doi.org/10.1126/sciadv.adh7820>.

- [21] S. Y. Al-nami, E. Aljuhani, I. Althagafi, H. M. Abumelha, T. M. Bawazeer, A. M. Al-Solimy, Z. A. Al-Ahmed, F. Al-Zahrani, and N. El-Metwaly, "Synthesis and Characterization for New Nanometer Cu(II) Complexes, Conformational Study and Molecular Docking Approach Compatible with Promising in Vitro Screening," *Arabian Journal for Science and Engineering*, vol. 46, no. 1, pp. 365–382, Aug. 2020, doi: <https://doi.org/10.1007/s13369-020-04814-x>.
- [22] M. S. Refat, A. Bayazeed, H. Katouah, R. Shah, M. Morad, M. Abualnaja, S. Alsaigh, F. Saad, and N. El-Metwaly, "In-silico studies for kinetin hormone and its alkaline earth metal ion complexes as anti-aging cosmetics; synthesis, characterization and ability for controlling collagen-inhibitors," *Journal of molecular structure*, vol. 1232, pp. 130041–130041, May 2021, doi: <https://doi.org/10.1016/j.molstruc.2021.130041>.
- [23] R. Shah, H. Katouah, A. A. Sedayo, M. Abualnaja, M. M. Aljohani, F. Saad, R. Zaky, and N. El-Metwaly, "Practical and computational studies on novel Schiff base complexes derived from green synthesis approach: Conductometry as well as in-vitro screening supported by in-silico study," *Journal of Molecular Liquids*, vol. 319, p. 114116, Dec. 2020, doi: <https://doi.org/10.1016/j.molliq.2020.114116>.
- [24] A. Daina, O. Michielin, and V. Zoete, "SwissADME: a Free web Tool to Evaluate pharmacokinetics, drug-likeness and Medicinal Chemistry Friendliness of Small Molecules," *Scientific Reports*, vol. 7, no. 1, pp. 1–13, Mar. 2017, doi: <https://doi.org/10.1038/srep42717>.
- [25] I. Rojas, O. Valenzuela, F. Rojas, and F. Ortuño, *Bioinformatics and Biomedical Engineering*. Springer Science+Business Media, 2019. doi: <https://doi.org/10.1007/978-3-030-17935-9>.
- [26] P. Dierks, A. Pöpcke, O. S. Bokareva, B. Altenburger, T. Reuter, K. Heinze, O. Kühn, S. Lochbrunner, and M. Bauer, "Ground- and Excited-State Properties of Iron(II) Complexes Linked to Organic Chromophores," vol. 59, no. 20, pp. 14746–14761, Sep. 2020, doi: <https://doi.org/10.1021/acs.inorgchem.0c02039>.
- [27] F. Juliá, "Ligand-to-Metal Charge Transfer (LMCT) Photochemistry at 3d-Metal Complexes: An Emerging Tool for Sustainable Organic Synthesis," *ChemCatChem*, vol. 14, no. 19, Sep. 2022, doi: <https://doi.org/10.1002/cctc.202200916>.
- [28] A. M. May and J. L. Dempsey, "A new era of LMCT: leveraging ligand-to-metal charge transfer excited states for photochemical reactions," *Chemical Science*, vol. 15, no. 18, pp. 6661–6678, May 2024, doi: <https://doi.org/10.1039/D3SC05268K>.
- [29] Y. Lin, E. Bilotti, C. W. M. Bastiaansen, and T. Peijs, "Transparent semi-crystalline polymeric materials and their nanocomposites: A review," *Polymer Engineering & Science*, vol. 60, no. 10, pp. 2351–2376, Aug. 2020, doi: <https://doi.org/10.1002/pen.25489>.
- [30] M. D. Olawale, A. C. Tella, J. A. Obaleye, and J. S. Olatunji, "Synthesis, characterization and crystal structure of a copper-glutamate metal organic framework (MOF) and its adsorptive removal of ciprofloxacin drug from aqueous solution," *New Journal of Chemistry*, vol. 44, no. 10, pp. 3961–3969, 2020, doi: <https://doi.org/10.1039/d0nj00515k>.
- [31] H.-J. Böhm, "Prediction of binding constants of protein ligands: a fast method for the prioritization of hits obtained from de novo design or 3D database search programs," *Journal of Computer-Aided Molecular Design*, vol. 12, no. 4, pp. 309–309, 1998, doi: <https://doi.org/10.1023/a:1007999920146>.
- [32] P. Ertl and A. Schuffenhauer, "Estimation of synthetic accessibility score of drug-like molecules based on molecular complexity and fragment contributions," *Journal of Cheminformatics*, vol. 1, no. 1, p. 8, Jun. 2009, doi: <https://doi.org/10.1186/1758-2946-1-8>.
- [33] I. I. Ahmed Juvale, A. A. Abdul Hamid, K. B. Abd Halim, and A. T. Che Has, "P-glycoprotein: new insights into structure, physiological function, regulation and alterations in disease," *Heliyon*, vol. 8, no. 6, p. e09777, Jun. 2022, doi: <https://doi.org/10.1016/j.heliyon.2022.e09777>.
- [34] B. Tóth, P. Krajcsi, and R. Magnan, "Membrane transporters and transporter substrates as biomarkers for drug pharmacokinetics, pharmacodynamics, and toxicity/adverse events," *Biomarkers in Toxicology*, pp. 947-963, 2014., doi: <https://doi.org/10.1016/b978-0-12-404630-6.00056-7>.
- [35] D. H. Upton, C. Ung, S. M. George, M. Tsoli, M. Kavallaris, and D. S. Ziegler, "Challenges and opportunities to penetrate the blood-brain barrier for brain cancer therapy," *Theranostics*, vol. 12, no. 10, pp. 4734–4752, 2022, doi: <https://doi.org/10.7150/thno.69682>.
- [36] D. Balayssac, N. Authier, A. Cayre, and F. Coudore, "Does inhibition of P-glycoprotein lead to drug–drug interactions?," *Toxicology Letters*, vol. 156, no. 3, pp. 319–329, Apr. 2005, doi: <https://doi.org/10.1016/j.toxlet.2004.12.008>.
- [37] N. A. Meanwell, "The Influence of Bioisosteres in Drug Design: Tactical Applications to Address Developability Problems," *Topics in Medicinal Chemistry*, pp. 283–381, 2013, doi: https://doi.org/10.1007/7355_2013_29.
- [38] M. F. da Silva, A. B. S. F. dos Santos, V. de Melo Batista, É. E. da Silva Rodrigues, J. X. de Araújo-Júnior, and E. F. da Silva-Júnior, New drug discovery and development. In *Dosage Forms, Formulation Developments and Regulations* Academic Press (pp. 3-65).